Available online at www.sciencedirect.com
SCIENCE DIRECT
Catalysis Today 110 (2005) 26–37
CATALYSIS TODAY
www.elsevier.com/locate/cattod

Experiments and modeling of membrane microreactors

King Lun Yeung [a,*], Xiongfu Zhang [a], Wai Ngar Lau [a], Rosa Martin-Aranda [b]

[a] *Department of Chemical Engineering, the Hong Kong University of Science and Technology, Clear Water Bay, Kowloon, Hong Kong, PR China*
[b] *Departmento de Química Inorgánica y Química Técnica, Universidad Nacional de Educación a Distancia, C/Senda del Rey 9, 28040-Madrid, Spain*

Available online 19 October 2005

Abstract

Two types of membrane reactors, the packed-bed membrane reactor (PBMR) and catalytic membrane reactor (CMR) were successfully miniaturized. Zeolites were incorporated as catalyst for reaction and membrane for separation. The membrane microreactors were tested for Knoevenagel condensation reaction between benzaldehyde and ethyl cyanoacetate to produce ethyl 2-cyano-3-phenylacrylate. Supra-equilibrium conversion and high product purity were obtained from selective removal of water during the reaction. A simple computation model was developed to simulate the reaction in the multichannel membrane microreactor using kinetic data from batch reaction, correlated data from membrane separation and published transport data. The influence of reactor geometry (i.e. channel width and membrane location), membrane separation and catalyst properties were evaluated and the results compared well with experimental data. The information provided by the model suggests several ways of improving the reactor performance.

Keywords: Miniature reactor; Base catalysis; Knoevenagel condensation; Zeolite; Pervaporation

1. Introduction

Miniaturization of chemical engineering processes is motivated by the quest for clean and efficient on-site, on-demand and on-time, distributed production of chemicals. The reactor being the heart of chemical production process has received a lot of attention. It has been shown that miniaturization can improve heat and mass transfer by decreasing the diffusion distance within the microreactor and increasing the interfacial area per unit reactor volume [1]. Rapid mass and heat transfer rates were obtained even at laminar flow regime [2] making microreactor an excellent choice for fast or highly exothermic reaction systems. Microreactors can suppress formation of hot spots and prevent runaway reaction enabling safe operation under otherwise dangerous conditions [3–5]. The precise spatial and temporal control over temperature, residence time, fluid flow and mixing is another advantage of microreactors [6]. Miniaturization also benefits membrane processes. A large membrane area in a small compact unit is obtained by simply assembling small membrane pieces. This is important for inorganic membranes, which are often brittle and difficult to form. The small membrane size also avoids many of the problems that plague large membrane units such as deformation and cracks introduced during processing and operation. The shorter diffusion length means enhanced mass transfer rate and an improved membrane separation as shown by the zeolite micromembranes reported by Leung and Yeung [7].

Multifunctional reactors that combine reaction and separation in a single process unit offer advantages in performance and operation. The selective removal of one or more products during reaction benefits reactions that are constrained by unfavorable thermodynamics. Supra-equilibrium conversion, improved selectivity and product purity are some of the observed benefits [8]. Membrane reactor also helped prevent catalyst poisoning and deactivation by removing undesirable byproducts from the reaction [9]. This work investigates the miniaturization of a packed-bed membrane reactor and catalytic membrane reactor for Knoevenagel condensation reaction of benzaldehyde and ethyl cyanoacetate. Zeolite catalysts and membranes are used to catalyze the reaction and

* Corresponding author. Tel.: +852 2358 7123; fax: +852 2358 0054.
E-mail address: kekyeung@ust.hk (K.L. Yeung).

0920-5861/$ – see front matter © 2005 Elsevier B.V. All rights reserved.
doi:10.1016/j.cattod.2005.09.020

Nomenclature

C	concentration of benzaldehyde (mol m^{-3})
$[C_7H_6O]$	concentration of benzaldehyde (M)
d	depth of channel (μm)
D	diffusion coefficient of bulk fluid ($m^2\ s^{-1}$)
D_{eff}	effective diffusivity of the catalyst ($m^2\ s^{-1}$)
[ECA]	concentration of ethyl cyanoacetate (M)
k	kinetic constant ($m^3\ mol^{-1}\ s^{-1}$)
l	channel length (mm)
r	rate of benzaldehyde conversion per unit catalyst surface area (mol $m^{-2}\ s^{-1}$)
S_a	surface area per unit mass of catalyst ($m^2\ g^{-1}$)
T	reaction temperature (K)
U_m	mean velocity ($m\ s^{-1}$)
U_z	fluid velocity along the z-axis ($m\ s^{-1}$)
w	channel width (μm)
x	radial dimension (m)
y	radial dimension (m)
z	dimension along channel length (m)

Greek letters

ΔP	pressure drop in microchannel (Pa)
ΔP_m	pressure drop across the zeolite membrane (Pa)
ρ	catalyst density ($g\ m^{-3}$)

separate the water byproduct. Zeolite and molecular sieve materials were incorporated as catalyst [10–13], membrane [7,14,15] and structural material [16] in miniature chemical devices such as microreactors and microseparators [17,18]. A recent review by Coronas and Santamaria [19] summarized the use of zeolite films in micro-scale applications. Very precise and localized addition of zeolite materials was obtained using new preparation techniques with a clear demonstration of direct engineering of the deposited zeolite's microstructure and chemistry [17,18]. Membrane microreactors using zeolite catalysts and membranes were successfully designed and fabricated. Reactions conducted in these membrane microreactors included Knoevenagel condensation [13,20,21] and selective oxidation reactions [22]. Supra-equilibrium conversion was obtained in the former, while the latter displayed improved performance against catalyst deactivation.

Computational modeling and simulation are important tools for the design of microreactor systems [23]. Microfluidic calculations provide invaluable information for designing the architecture of the microreactor [24]. Detailed simulation and modeling studies conducted by various researchers [25,26] have provided important insights to the reaction behavior in a microsystem environment. In this work, we present a simple reactor model for predicting the behavior of the Knoevenagel condensation reaction in a multichannel membrane microreactor. The kinetic data for the model were obtained from separate batch experiments, while the membrane separation was conducted on the actual miniature membrane unit and the transport data were taken from the literature. The influence of reactor geometry (i.e. channel width and membrane location), membrane separation and catalyst properties were evaluated and the results compared well with experimental data. The information provided by the model suggests several ways of improving the reactor performance.

2. Experiments

2.1. Microreactor design and fabrication

The microreactor design emphasizes on flexibility and ease of use. It consists of a microreactor plate and stainless steel housing. The plate contains the microfluidic components, the active catalyst and the separation membrane, while the housing unit provides a convenient interface between the microreactor and the macroscale laboratory environment. The detailed description of the microreactor housing can be found in the work of Lai et al. [21]. The modular design enables the rapid fabrication and testing of different microreactor architectures, catalysts and membranes. Fig. 1 summarizes the preparation and test procedures for the two types of multichannel microreactor plates. The membrane–catalyst plates consist of catalyst-coated microchannels with a membrane layer deposited on the back of the plate. The catalytic membrane plates have a layer of catalytic membrane deposited on the wall of the microchannels where the reaction and separation can take place simultaneously.

2.1.1. Membrane–catalyst plates

The *porous multichannel plates* were made from porous SS-316L plates (0.2 μm) purchased from Mott metallurgical corporation. Stainless steel was selected because of its good compatibility with most reactions, excellent machinability and low cost. Thirty-five straight channels measuring 300 μm wide, 600 μm deep and 25 mm long were cut into the 1 mm thick, 25 mm × 25 mm porous plates using electrical discharge micromachining (EDM, AGIE Wirecut 120). After fabrication, the plates were cleaned with detergent and rinsed with water to remove oils and dirt. The plates were further treated with dilute 0.05 M nitric acid to remove rust, before rinsing with deionised, distilled water and ethanol.

Zeolite membranes were grown on the back of the multichannel plate by pre-seeding the stainless steel with zeolite nanocrystals. The 100 nm Sil-1 and 150 nm NaA seeds were used to prepare ZSM-5 and NaA membranes, respectively. Mercapto-3-propyltrimethoxysilane was first coated on the back of the plate to provide the seeds with a strong anchor to the surface. The plate was then brushed with a water mixture containing 1 wt.% zeolite seeds. The process was repeated four times to obtain a uniform seed coating. After drying, the seeded plate was heat-treated at 523 K for 24 h to ensure good adhesion of the seed layer. The ZSM-5 zeolite membranes were grown from a synthesis solution containing a molar composition of 80 SiO_2:4 Al_2O_3:5 Na_2O:1 tetrapropylammonium hydroxide (TPAOH):20,000 H_2O. The aluminum hydroxide prepared by dissolving aluminum sulfate (98+%, Aldrich) in excess ammonium hydroxide solution was filtered, washed and weighed, before adding to a solution of 0.04 M sodium

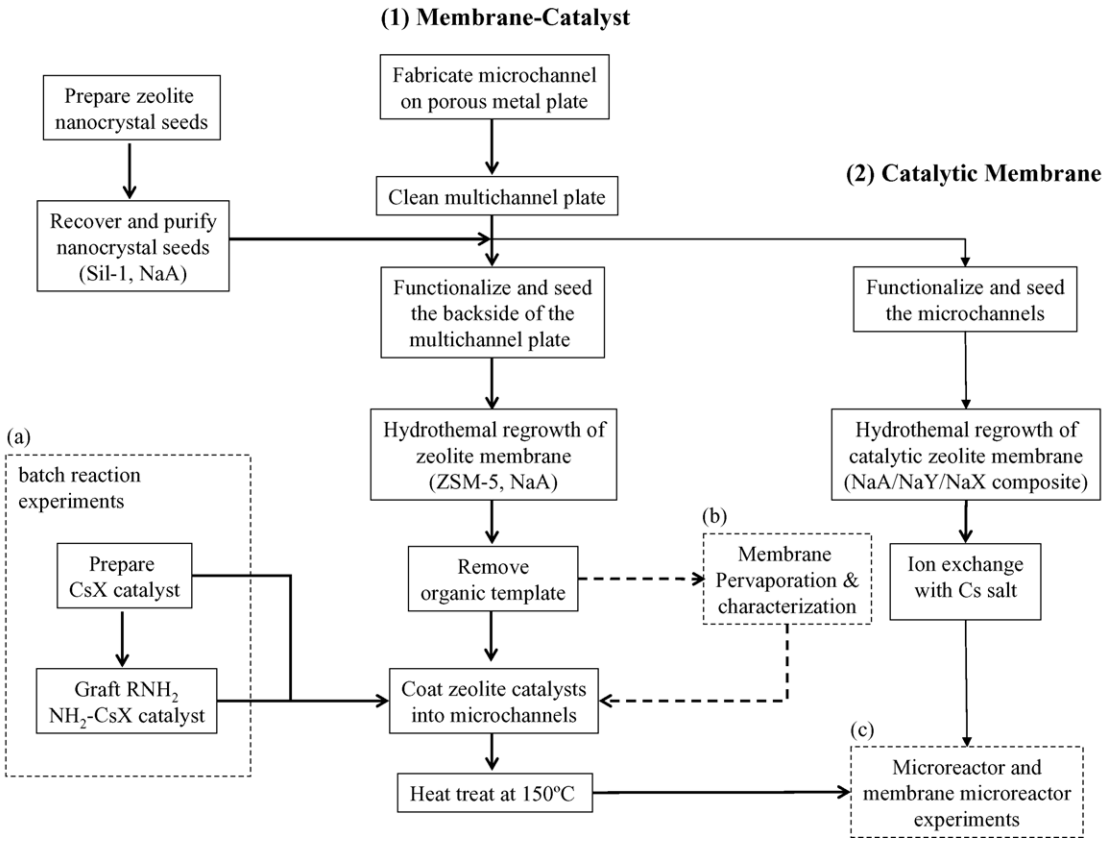

Fig. 1. Process flow diagram for the preparation of membrane–catalyst and catalytic membrane plates.

hydroxide (99%, Aldrich) and 0.014 M TPAOH (1 M, Aldrich). Tetraethyl orthosilicate (TEOS, 98%, Aldrich) was then added with vigorous stirring to obtain a clear synthesis solution. The porous multichannel plate was placed horizontally in a Teflon vessel with the seeded surface facing downward to prevent powder deposition on the growing zeolite film. The growth was conducted in an autoclave at a temperature of 453 K. The NaA membrane was grown from a clear synthesis solution containing molar ratio of 5 SiO_2:1 Al_2O_3:52 Na_2O:3750 H_2O at a temperature of 373 K. The silica precursor was obtained by hydrolysis of TEOS, while sodium aluminate purchased from Riedel-de Haën provided the alumina source. The pH of the synthesis mixture was adjusted using sodium hydroxide (99%, Riedel-de Haën).

After membrane deposition, the plate was rinsed with distilled deionised (DDI) water and dried prior to weighing and inspection with an optical microscope to determine the amount and coverage of the zeolite deposit. The membrane was also examined by X-ray diffraction (XRD, Philips 1080) and scanning electron microscopy (SEM, JEOL 6300). X-ray photoelectron spectroscopy (XPS, Physical Electronics PHI 5600) was conducted on the membrane samples to determine their compositions. The membranes were tested for pervaporation of water/benzaldehyde mixtures (Fig. 1(b)). The liquid solution was fed at a flowrate of 1 ml/h and the membrane pervaporation was conducted at a temperature of 373 K and a vacuum pressure of 16.7 kPa. The retentate was cooled to room temperature and collected in a sample vial, whereas the permeate stream was condensed and collected in a liquid nitrogen trap. The retentate and permeate were weighed and analyzed by gas chromatography (GC, HP 5890). The permeate flux, P (kg h^{-1} m^{-2}) was calculated. The selectivity of the membrane separation, α was calculated from the composition of the liquids collected from the retentate and permeate:

$$\alpha = \frac{(Y_{H_2O}/Y_{organics})}{(X_{H_2O}/Y_{organics})} \quad (1)$$

where Y_i and X_i are the weight fraction of component i in the permeate and retentate, respectively.

Catalysts were deposited onto the microchannels by the following procedures. A thin layer of polydiallyldimethyl ammonium chloride (PDAMAC, Aldrich) was coated onto the microchannel from a 20 wt.% PDAMAC solution. The coating was applied using a brush and was blown-dried with compressed air. The multichannel plate was pressed face down against a clean glass plate. Two milliliter of dilute catalyst suspension in water was placed near the channel openings and drawn into the microchannel with the aid of a light suction. The negatively charged zeolite particles were deposited onto the positively charged PDAMAC-coated microchannel walls. After drying at room temperature, the plate was heat-treated at 423 K for 24 h to obtain a good catalyst adhesion. The amount of

deposited catalyst was determined from the weight difference between the coated and uncoated porous multichannel plate. Visual inspection, using the optical microscope and detailed imaging by SEM provided information on the catalyst coverage within the microchannels.

Two zeolite catalysts were prepared from Faujasite X zeolite powder purchased from Aldrich Chemicals (Fig. 1(a)). The zeolite powder was ground, sieved and calcined to obtain a uniform catalyst powder free of moisture and adsorbed organic contaminants. The Cs-exchanged X (CsX) zeolite was prepared by ion-exchange of NaX powder with 0.5 M cesium chloride (98+%, Sigma) solution at 353 K for 6 h. This procedure was repeated three times to obtain a maximum Cs/Si loading of 0.32. An active zeolite catalyst was obtained after pretreatment in air at 673 K for 4 h. NH_2–CsX was prepared by grafting 3-aminopropyl-trimethoxysilane (APTS, 97%, Aldrich) on CsX zeolite. The structure and composition of the zeolite catalysts were analyzed and reported in a recent publication [13]. The kinetic data was obtained from the batch reaction experiments using 1 wt.% catalyst powder (0.031 g) and a stoichiometric mixture of 14 mmol of benzaldehyde (99%, RDH) and 14 mmol of ethyl cyanoacetate (98+%, Aldrich). Solvent was not used and the reaction was conducted under nitrogen atmosphere to prevent the formation of undesired byproducts (e.g., benzoic acid). The stirring rate was kept at 1000 rpm to eliminate the external mass transfer resistance. Samples were taken at intervals for analysis by gas chromatography. The GC was equipped with a 60 m phenylsilicone capillary column (Alltech) and a flame ionisation detector.

2.1.2. Catalytic membrane plates

The microchannels were uniformly seeded with 150 nm NaA nanocrystals and placed in a synthesis solution containing molar ratio of 5 SiO_2:1 Al_2O_3:52 Na_2O:3750 H_2O. The synthesis was conducted at 373 K for 10 h and was repeated three times to produce a 6 μm thick layer of NaA membrane on the wall of the microchannels. A final layer of Faujasite was deposited from a solution with a composition of 5 SiO_2:1 Al_2O_3:56 Na_2O:2500 H_2O at a synthesis temperature of 373 K for 10 h. After each deposition steps, the plate was weighed and inspected with an optical microscope. The sample was ion-exchanged with 0.5 M cesium chloride solution at 353 K for 6 h. This was repeated three times to obtain a Cs-exchanged Faujasite–NaA catalytic membrane. The sample was analyzed by XRD and SEM after the reaction experiment.

2.2. Microreactor performance study

The microreactor plate was placed in the stainless steel reactor housing. The reactor contained an inlet and outlet for the reactants and products, as well as a vacuum feedthrough for the membrane permeate. A Pyrex glass cover completed the reactor assembly. The transparent cover provided a window for monitoring the progress of the reaction in addition to observing fluid flow and mixing. A temperature programmer unit (Omega) controlled the reactor temperature through a thermocouple inserted near the plate. A copper block fitted with twin heating cartridges was used to keep the temperature at a desired level. Water removal by membrane pervaporation requires vacuum. The vacuum feedthrough was located directly beneath the microreactor plate and was connected to a vacuum pump (Barnant Company, Edwards Company) through a liquid nitrogen trap where the permeate vapor was condensed and collected.

A 25 ml syringe (Hamilton) was filled with an equimolar solution of benzaldehyde and ethyl cyanoacetate. The preheated reactor (i.e. 373 K) was manually filled with the reactant solution, taking care that no bubbles were formed during the process. Once the reactor was filled, the syringe was transferred to the syringe pump and the liquid was fed at a fixed rate (i.e. 0.2–12 ml/h). The microreactor data was obtained with the permeate vacuum closed and the reaction solution was collected from the reactor outlet at fixed time intervals until a steady state condition was reached. For the membrane microreactor operation, the vacuum was turned on and samples were obtained from both the reactor and permeate outlets. The quenched samples were filtered and diluted with *tert*-butyl methyl ether (MTBE, 99.8%, Fluka) and injected into the gas chromatograph. Three GC measurements were made for each sample and the concentration of the reactants and products were determined from a calibration curve prepared from standard solutions containing known quantities of benzaldehyde, ethyl cyanoacetate and ethyl 2-cyano-3-phenylacrylate (98%, TCI). Samples collected from the permeate outlet were also analyzed by TOC analyzer (TOC 500, Shimadzu) after dilution with DDI water to determine the amount of organic carbon.

3. Microreactor model

The reaction in the microchannel was described by a simple three-dimensional reactor model. The model assumes an isothermal, steady state operation condition. Eqs. (2) and (3) are the differential material balance equations for the bulk fluid in the channel and across the catalyst layer, respectively:

$$U_z \frac{\partial C}{\partial z} = \frac{\partial}{\partial x}\left(D\frac{\partial C}{\partial x}\right) + \frac{\partial}{\partial y}\left(D\frac{\partial C}{\partial y}\right) \tag{2}$$

$$\frac{\partial}{\partial x}\left(D_{\text{eff}}\frac{\partial C}{\partial x}\right) + \frac{\partial}{\partial y}\left(D_{\text{eff}}\frac{\partial C}{\partial y}\right) + r\rho S_a = 0 \tag{3}$$

where C is the concentration of benzaldehyde reactant (mol m^{-3}), D, the diffusivity of the bulk fluid in the channel (m^2 s^{-1}), D_{eff}, the effective diffusivity in the catalyst layer (m^2 s^{-1}), x, y and z, the dimensions along the width, depth and length of the channel (m), r, the rate of disappearance of benzaldehyde per unit area of catalytic surface (mol s^{-1} m^{-2}), S_a, the surface area per unit mass of catalyst (m^2 g^{-1}), ρ, the density of catalyst (g m^{-3}) and U_z is the fluid velocity along the z-axis (m s^{-1}).

The reaction data for the Knoevenagel condensation of benzaldehyde and ethyl cyanoacetate was obtained from the

batch reaction experiments and fitted to a second-order reversible reaction kinetic equation. The kinetic data included contributions from the intra-particle diffusions of reactants and products in the zeolite pores. Since the same catalyst was used in the microreactor experiments, it is not necessary to separately measure the intra-particle diffusion in the zeolite catalyst. This makes both the experiment and computation simpler. The equilibrium conversion was determined experimentally, since the thermodynamic data for ethyl 2-cyano-3-phenylacrylate product was not available.

The transport mechanisms are considered to be convection along the flow direction and diffusion along the traverse directions. The fluid flow in the microchannel is laminar and the axial diffusion in the flow direction was neglected because its contribution is small when compared to the reactant flow. The fluid transport through the catalyst layer is given by the inter-particle diffusion (D_{eff}) and possesses a relative diffusivity of about 3×10^{-10} m^2 s^{-1} for the loosely packed layer of catalyst particles. This is roughly twenty percent of the value of the bulk diffusivity. The fluid entering the microreactor has a uniform concentration and a fully developed flow where the velocity profile is invariant along the flow axis. The flow profile in the microchannel is described by:

$$U_z = U_m \left[1 - \left(\frac{2y}{h}\right)^n\right]\left[1 - \left(\frac{2x}{w}\right)^m\right] \quad (4)$$

where U_z is the velocity along the z-axis (m s^{-1}), U_m, the mean velocity (m s^{-1}), x and y, the transverse coordinates (m), n, given by $2.0 + 3(\alpha' - 1/3)$ for $\alpha' > 1/3$ and m is given by $1.7 + 0.5\,\alpha'^{-1.4}$ [27]. In the model, the microchannel was approximated by a rectangular cross-section of similar peripheral area. It was also assumed that the fluid is incompressible that its properties remain unchanged during the reaction and the pressure drop along the channel is negligible.

The membrane was located at the bottom of the microchannel separated by a 300 μm thick layer of porous stainless steel. During the membrane operation, the fluid diffuses across the stainless steel and permeated through the membrane. The diffusivities though the porous stainless steel was estimated to be roughly half that of the bulk diffusion from the flux measurements. The membrane was modeled as a boundary condition in the system. It has been suggested that thermodynamic calculation could be used to predict the permeation flux and selectivity of the zeolite membranes. However, a simple correlation based on the actual experimental data is more accurate and convenient.

The partial differential equations (Eqs. (2) and (3)) were integrated along the z-axis to calculate the benzaldehyde concentration profile in the microreactor. The concentration profiles of the ethyl cyanoacetate, ethyl 2-cyano-3-phenylacrylate and water were calculated from the mass balance. The governing equations were solved using Femlab™. The microchannel was partitioned into approximately 1600 finite element cells using an adaptive mesh. The mesh was smaller and denser at the proximity of the catalyst layer where the reaction took place in order to ensure a more accurate calculation of the concentration profile along the microchannel. The results for the single microchannel were scaled-up to the 35 channels microreactor for comparison with the experimental data. A simple but accurate model is useful and convenient for studying the effects of reactor geometry, catalyst and membrane properties and reaction conditions on the microreactor performance.

4. Results and discussion

4.1. Microreactor plates

The microreactor plates have three functional elements namely, the flow architecture, the active catalyst and the separation membrane. The membrane–catalyst plates consist of multiple microchannels coated with catalysts for reaction and a membrane deposited at the back of the plate separated from the microchannels by a layer of porous stainless steel. The catalytic membrane plates have composite layers of NaA–Faujasite membrane deposited on each microchannel that allow simultaneous reaction and separation. The separation properties of NaA and ZSM-5 membranes, as well as the reaction kinetics of CsX and NH_2–CsX catalysts were evaluated to provide data for modeling the microreactor performance.

4.1.1. Membrane–catalyst plates

The SEM pictures in Fig. 2a show the top and cross-section views of a typical multichannel microreactor plate. The microchannels cut by EDM process are evenly spaced and the channel size corresponding to the diameter of the wire used in the machining. Each of the microchannel has a volume of 4.5 μl giving the entire multichannel plate a total volume of 0.16 ml. The catalyst–membrane plate shown in Fig. 2b and c consists of CsX-coated microchannels (Fig. 2b) and a NaA membrane grown on the back of the porous multichannel plate (Fig. 2c). It is clear from Fig. 2b that there is less than monolayer catalyst coverage at 0.01 g CsX/cm^3 reactor volume. The individual zeolite catalyst particles are roughly spherical in shape with an average particle size of about 2 μm. The catalyst particles are trapped in the grooves and crevices of the porous stainless steel. The 6 μm thick NaA membrane shown in Fig. 2c is the result of three-repeated synthesis. The deposited membrane is polycrystalline and made of intergrown zeolite crystals. The pyramidal-shaped crystals are the results of the (1 1 1)-oriented cubic NaA zeolites. The structural characteristics and chemical properties of the deposited zeolite are dictated by the synthesis composition and conditions [28]. The growth environment has also been shown to affect the zeolite's crystal habit and film orientation [29], which could significantly affect the transport properties across the zeolite layer.

Two types of catalyst–membrane plates using 30 μm ZSM-5 and 6 μm NaA membranes were tested. A 30 μm thick ZSM-5 is needed to produce a defect-free membrane on the porous stainless steel. Analysis indicated that the well-intergrown ZSM-5 membranes possessed a (0 0 2) film orientation and consisted of interlocked columnar ZSM-5 crystals. Helium leak

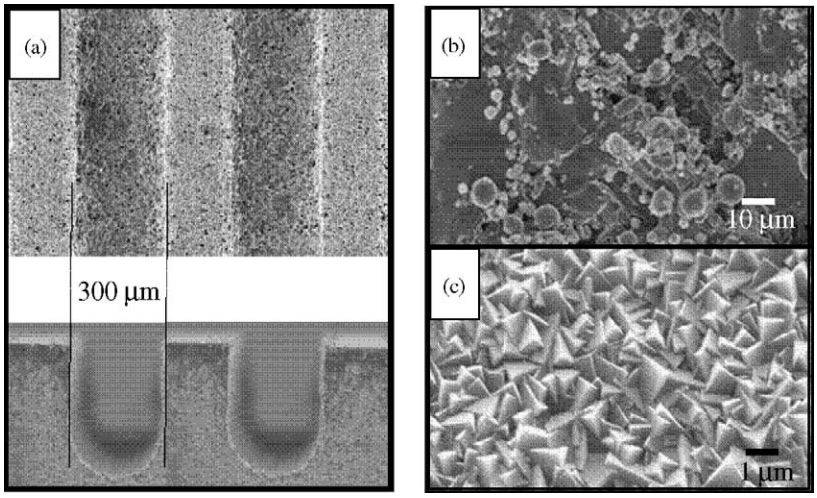

Fig. 2. Scanning electron microscope pictures of (a) top and cross-section views of a membrane–catalyst plate with (b) 0.01 g/cm^3 CsX catalysts coated on the microchannels and (c) 6 μm thick NaA separation membrane.

test showed that prior to the removal of the organic template molecules (i.e. TPA^+) trapped within the zeolite pores, the membrane was impermeable. Elemental analysis showed that the membrane has a Si/Al ratio of 30. The permeate flux (P) and separation factor (α) for water is plotted in Fig. 3a as a function of water concentration in the benzaldehyde solution. The permeate flux across the ZSM-5 membrane increases linearly with water concentration. A very high separation factor of 240,000 is obtained at low water concentration of 1 wt.%, which decreases to a lower value of 50,000 at 5 wt.% water. Unlike the ZSM-5 membrane, both the permeate flux and membrane selectivity of the 6 μm thick NaA membrane are constant and independent of water concentration as shown in Fig. 3b. The thinner NaA membrane exhibits nearly an order of magnitude higher permeate flux compared to the ZSM-5 membrane, while maintaining a high separation factor of 150,000 for water.

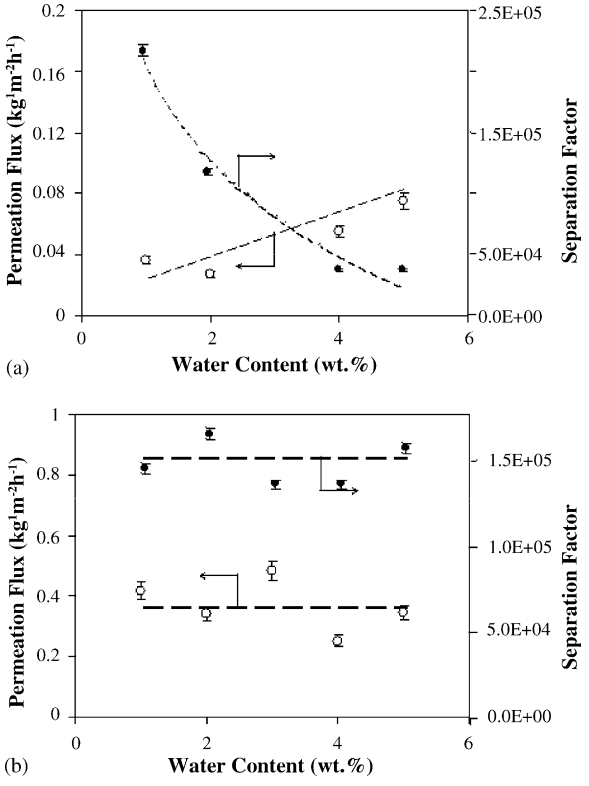

Fig. 3. Water permeation flux and separation factor for (a) 30 μm ZSM-5 and (b) 6 μm NaA membranes plotted as a function of water concentration in benzaldehyde (T = 373 K, P = 84.7 Pka, q_f = 1 ml/h). Please note the lines were added to guide the eyes.

The two catalysts used in the membrane–catalyst plates are CsX and NH_2–CsX zeolite catalysts. CsX was prepared by ion-exchanging NaX with cesium ion and possessed an average particle size of 1.9 μm, a BET surface area of 400 m^2/g and a Cs/(Na + Cs) ratio of 0.63. The NH_2–CsX prepared by further grafting aminopropyl groups to CsX has a smaller surface area of 200 m^2/g and contains N/Si ratio of 3.1. The data from the batch reaction experiments fit a second-order, reversible reaction equation (Eq. (5)):

$$r = k\left(C_a C_b \frac{C_c C_d}{K_e}\right) \tag{5}$$

where C_i is the concentration of species i (mol m^{-3}), k, the reaction rate constant (m^3 mol^{-1} s^{-1}), $K_e = \frac{C_{ce}C_{de}}{C_{ae}C_{be}}$, the equilibrium constant with C_{ie} being the equilibrium concentration of species i (mol m^{-3}). The reaction rate constants for CsX catalyst at 363, 393 and 413 K are 3.7×10^{-8}, 4.6×10^{-8} and 7.8×10^{-8} m^3 mol^{-1} s^{-1}, respectively. This gives activation energy of 17.4 kJ mol^{-1}, which is smaller than the 34–41 kJ mol^{-1} reported by Corma et al. [30] for X zeolites. The NH_2–CsX catalyst is roughly three times more active than the CsX catalyst and has activation energy of about 21 kJ mol^{-1}.

4.1.2. Catalytic membrane plates

Fig. 4a displays the SEM picture of a catalytic membrane plate. The Cs-exchanged Faujasite–NaA catalytic membrane was uniformly deposited on the microchannel wall creating 35

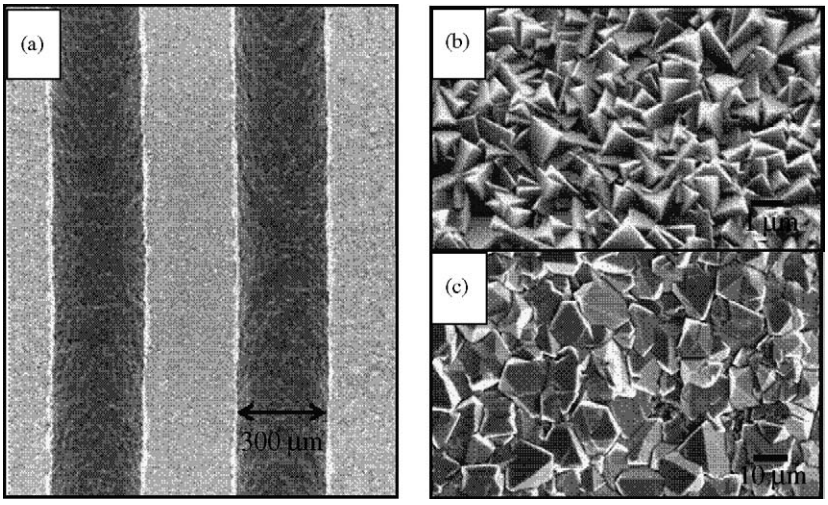

Fig. 4. Scanning electron microscope pictures of (a) top view of a catalytic membrane plate with a composite micromembrane deposited on each microchannel consisting of (b) 6 μm thick NaA and (c) 4 μm thick Faujasite.

discrete micromembrane units. Six microns thick NaA micromembrane was first deposited on the microchannels (Fig. 4b) using the same synthesis composition and procedure as the membrane grown on the backside of the catalyst–membrane plate shown in Fig. 2c. The NaA micromembranes give a water flux of 0.3 kg m^{-2} h^{-1} at a selectivity of 120,000 for benzaldehyde solution containing 2 wt.% water. These values are comparable to the results given in Fig. 3b for a similar thickness NaA membrane. A slight increase in pH enabled the deposition of a final layer of Faujasite zeolites shown in Fig. 4c. The bipyramidal crystals shown in the figure are characteristic shape of Faujasite zeolites. Both zeolite X and Y are deposited forming the four microns thick, intergrown, polycrystalline catalyst layer. Following ion-exchange of cesium, the final catalytic membrane consists of composite layers of NaA membrane and the Faujasite catalyst.

4.2. Microreactor performance

4.2.1. Membrane–catalyst plates

Reaction tests conducted on bare multichannel plate showed that stainless steel was inactive for Knoevenagel condensation of benzaldehyde and ethyl cyanoacetate. However, a slight production of benzoic acid was observed at reaction temperatures above 373 K. Multichannel plates coated with ZSM-5 and NaA zeolite membranes were also inactive for the reaction. Fig. 5a and b plots the concentrations of benzaldehyde, ethyl cyanoacetate and ethyl 2-cyano-3-phenylacrylate as a function of residence time for the microreactor and membrane microreactor, respectively. The membrane–catalyst plate had 0.03 g CsX/cm^3 of evenly deposited in the microchannels and employed a 30 μm thick ZSM-5 membrane. The plots shown in Fig. 5 compare the experimental data and modeling results. The model uses the reaction rate equation derived from the batch reaction experiments for the CsX catalyst and the correlated separation data for ZSM-5 membrane. Table 1 summarizes the experimental and model values for the microreactor and membrane microreactor. Despite the various simplifications, it is clear that the computational model give an adequate description of the microreactor and membrane microreactor processes.

Fig. 5a shows that the concentrations of benzaldehyde and ethyl cyanoacetate at the microreactor outlet decrease with

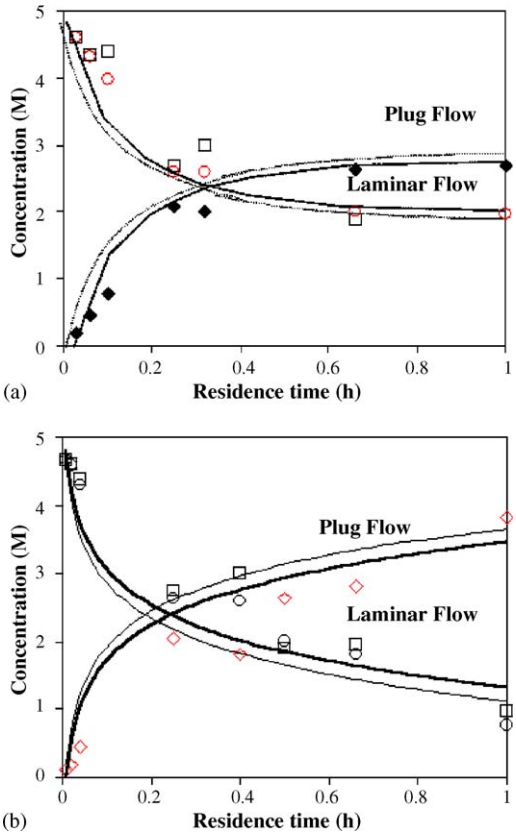

Fig. 5. Plots of the molar concentrations of reactants and products in the reactor outlet of (a) microreactor and (b) membrane microreactor for different residence times. (T = 373 K, $[C_7H_6O]_0$ = 4.8 M, $[ECA]_0$ = 4.8 M, catalyst loading = 0.01 g/cm^3 CsX, membrane = 30 μm ZSM-5, ○: benzaldehyde, □: ethyl cyanoacetate, ◇, ◆ ethyl 2-cyano-3-phenylacrylate, dark line: laminar flow model, grey line: plug flow model).

Table 1
Experimental and model values for microreactor and membrane microreactor

Parameter	Units	Experimental value	Modeling value
Channel length, l	(mm)	25	25
Channel width, w	(μm)	300	150–900
Channel depth, d	(μm)	600	600
Catalyst layer width, δ	(μm)	5–150	5
Catalyst density, ρ	(g m^{-3})	1.6×10^6	1.6×10^6
Catalyst crystal size, R	(μm)	2–4	2–4
Residence time, τ	(h)	0–1	0–10
$[C_7H_6O]_0$	(mol m^{-3})	4789	4789
Stoichiometric ratio of reactants	–	1	1
Diffusion coefficient			
Bulk channel [31,32], D	(m^2 s^{-1})	–	2×10^{-9}
Catalyst layer [33], D_{eff} at $R = 2$ μm	(m^2 s^{-1})	–	3×10^{-11}
Catalyst layer [34], D_{eff}	(m^2 s^{-1})	–	$3 \times 10^{-11} \times 2/R$

residence time as the reaction conversion increases. The benzaldehyde conversion is higher than ethyl cyanoacetate because of the side reaction to benzoic acid. Ethyl 2-cyano-3-phenylacrylate and water are produced by the reaction. The model calculated by assuming a laminar flow profile in the microchannels is in better agreement with the experimental data compared to a plug flow model. The model predicts that the equilibrium conversion is the maximum allowable conversion in the microreactor. The Knoevenagel condensation reaction is constrained by unfavorable thermodynamic equilibrium and the continuous and selective removal of water byproduct from the reaction is expected to improve the conversion. Indeed, a higher conversion with a better product yield is evident by the lower reactant and higher product concentrations in Fig. 5b for the membrane microreactor. Supra-equilibrium conversion is obtained as water is selectively removed by pervaporation through the ZSM-5 membrane. The figure shows that the experimental data and model prediction are in good agreement.

4.2.2. Influence of microchannel width

The microchannel is the simplest architectural element in the microreactor design and even today's most complex microreactor is essentially an assembly of interconnected microchannels. The microchannel geometry is defined by the width (w) and depth (d) of its cross-section and by the length (l) of the channel. In this study, the depth of the microchannel was fixed at 600 μm and the channel length at 25 mm. Fig. 6a shows the ethyl 2-cyano-3-phenylacrylate product yield as a function of residence time for different channel widths. The experimental data for the 30 μm ZSM-5 membrane-0.03 g/cm^3 CsX catalyst plate with a channel width of 300 μm is included in the plots for comparison. It can be seen that there is a good agreement between the model prediction and experimental data. The model predicts that narrower channels would give higher conversion because both the catalyst loading and membrane area per unit reactor volume is larger. The reaction also benefits from the shorter diffusion length. However, a narrower channel will experience more severe pressure drop (ΔP), which increases in inverse proportion to the cube of the channel width. Calculations showed that pressure drop would be a major problem for channel widths narrower than 100 μm, posing a severe limitation on the microreactor operation. Experiments also showed that bubble formation could be a problem at the reaction condition even for the wider 300 μm channels.

4.2.3. Influence of membrane separation

The selective removal of water by membrane pervaporation can eliminate the thermodynamic constraints imposed by the equilibrium reaction. It is expected that improvements in the membrane separation will enhance the reactor performance. Two membrane–catalyst plates were prepared, one with a 30 μm thick ZSM-5 and the other a thinner 6 μm NaA membranes. It has been established that the NaA membrane has an order of magnitude higher flux compared to the ZSM-5 membrane (Fig. 3). Both plates were coated with 0.01 g CsX catalyst/cm^3 reactor and tested for the reaction at 373 K. It can be seen from the plots in Fig. 6b that when operated as a microreactor, both plates give a comparable product yield. This is reasonable since the membranes are inert and do not participate in the reaction. The figure also shows that the membrane microreactors consistently outperformed the microreactor. Despite the improvements seen in the membrane microreactors, the best yield is still below the expected equilibrium value of 72%. Operated as a membrane microreactor, the plate coated with the thinner NaA performs better. This is especially true at short residence time where the faster transport rate across the NaA membrane was able to remove all the water produced, which the thicker ZSM-5 was not able to do. This advantage disappears at longer residence time as shown in the figure. Calculations indicated that the ZSM-5 membrane is capable of removing >90% of the water produced by the reaction at residence times longer than 0.1 h. This observation is consistent with the model prediction showing that despite the large improvement in membrane separation performance, there is only an incremental increase in the conversion between the ZSM-5 and NaA membrane-0.01 g/cm^3 CsX catalyst plates. The model also predicts that no significant increase in the product yield will be observed even if

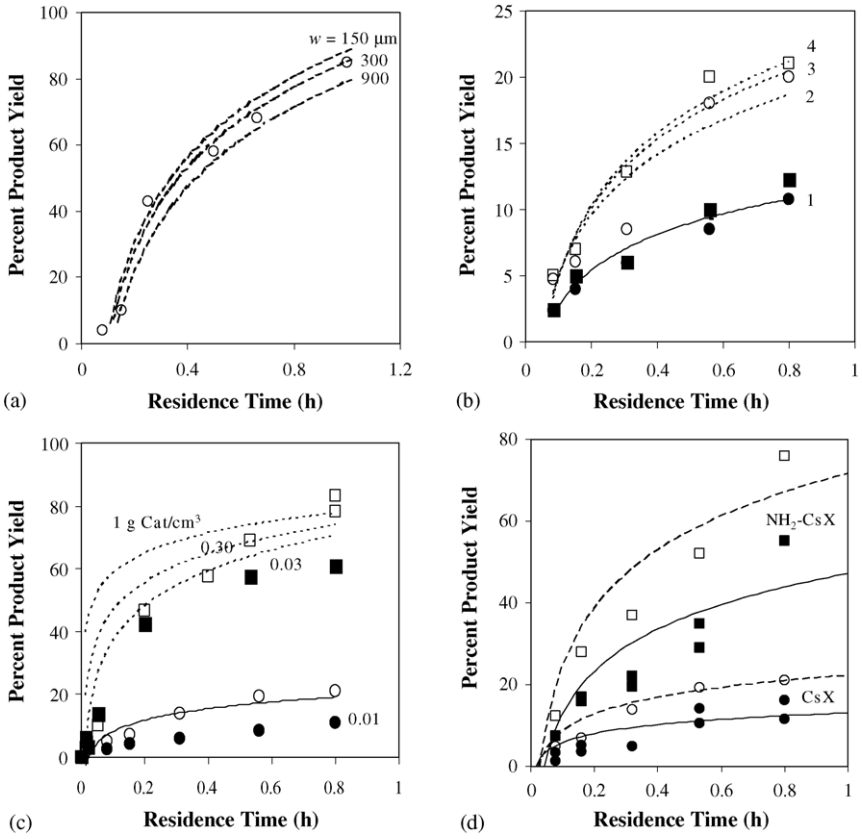

Fig. 6. (a) Percent product yield in a membrane microreactor as a function of residence time for different channel widths of 150, 300 and 900 μm. (T = 373 K, $[C_7H_6O]_0$ = 4.8 M, $[ECA]_0$ = 4.8 M, catalyst loading = 0.01 g/cm^3); (b) percent product yield as a function of residence time for different membrane permeation flux: (1) 0, (2) 0.03, (3) 0.3, and (4) 3 kg m^{-2} h^{-1} (T = 373 K, $[C_7H_6O]_0$ = 4.8 M, $[ECA]_0$ = 4.8 M, catalyst loading = 0.01 g/cm^3 CsX, ●, ○: 30 μm ZSM-5 membrane, ■, □: 6 μm NaA membrane); (c) percent product yield as a function of residence time for different CsX catalyst loadings. (T = 373 K, $[C_7H_6O]_0$ = 4.8 M, $[ECA]_0$ = 4.8 M, catalyst loading: ●, ○: 0.01 g/cm^3 CsX and ■, □: 0.03 g/cm^3 CsX, membrane = 6 μm NaA); (d) percent product yield as a function of residence time for 0.01 g/cm^3 CsX (●, ○) and 0.01 g/cm^3 NH_2–CsX (■, □) (T = 373 K, $[C_7H_6O]_0$ = 4.8 M, $[ECA]_0$ = 4.8 M, membrane = 6 μm NaA); please note that symbols represent the experimental data (solid symbols: microreactor, open symbols: membrane microreactors), while the lines are model prediction (solid lines: microreactor, dashed lines: membrane microreactor).

a membrane with 10 times better separation properties than NaA is used. This suggests that the membrane separation is not the limiting process in the membrane microreactor.

4.2.4. Influence of catalyst loading

A faster reaction can be obtained by simply increasing the catalyst loading. Fig. 6c plots the product yield as a function residence time for two NaA membrane–CsX catalyst plates with catalyst loadings of 0.01 and 0.03 g/cm^3. The figure shows a significant increase in the product yield for the microreactor with the higher catalyst loading. A supra-equilibrium conversion of 80% was obtained for the membrane microreactor with 0.03 g/cm^3 CsX loading. The model fits the two sets of experimental data well as shown in the figure. The model predicts that beyond the initial jump in the yield, the subsequent improvements are small and incremental especially at long residence time (Fig. 6c). The most significant effect of increasing reaction rate is that supra-equilibrium conversion is reached at a shorter residence time. This means higher production rates. However, we observed experimentally that the microchannels could only accommodate at most 0.03 g/cm^3 of catalysts.

Fig. 7a plots the product yield of a microreactor as a function of CsX loading. The reaction was run at 373 K at a residence time of 0.8 h. The model predicts that equilibrium conversion can be reached using as little as 0.045 g/cm^3 CsX catalysts at these reaction conditions. Constrained by the equilibrium, the maximum attainable conversion in the microreactor remains unchanged with the addition of more catalysts. However, the experiments show that the actual reaction conversion decreases when the catalyst loading in the microchannels increases to 0.1 and 0.3 g CsX/cm^3, as shown in the figure. It is observed that the flow in the microreactor is uniform for catalyst loadings of up to 0.03 g/cm^3 CsX. A closer inspection shows that at these catalyst loadings the microchannels are evenly coated with a thin layer of catalysts (Fig. 7b). The microchannels slowly filled-up as the catalyst loading increases (Fig. 7c) until eventually the microchannels are occupied with packed-beds of catalysts. This resulted in an erratic flow pattern in the microreactor with pulsed and oscillatory flow movements in the microchannels. At a catalyst loading of 0.3 g CsX/cm^3, flows to some of the microchannels are completely blocked and there is evidence of catalyst lost at high flow rates (>1 ml/h). This may explain

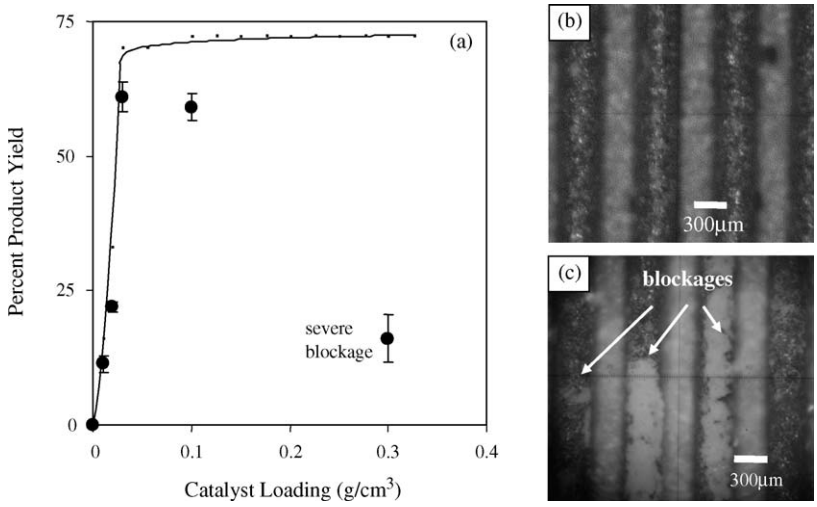

Fig. 7. (a) Plots of percent product yield as a function of CsX catalyst loading for a microreactor (T = 373 K, $[C_7H_6O]_0$ = 4.8 M, $[ECA]_0$ = 4.8 M, residence time = 0.8 h). The symbols and line represent the experimental and model data, respectively. Optical microscope pictures of microchannels coated with (b) 0.03 g/cm^3 and (c) 0.3 g/cm^3 CsX.

the eventual drop in the microreactor performance despite the increased catalyst loading.

4.2.5. Influence of reaction temperature

Increasing the reaction temperature benefits the Knoevenagel condensation reaction by increasing both the reaction rate and equilibrium conversion. The Arrhenius plot of the reaction is shown in Fig. 8a. There is a good agreement between the experiment and model at low temperatures, but above 373 K, the experimental results are lower than that are expected. This is due to the excessive bubble formation at temperatures above 373 K. Fig. 8b shows a normal microreactor operation at 373 K, while Fig. 8c displays the same reactor at 423 K. The ethyl cyanoacetate as well as water have relatively high vapor pressures and are easily vaporized during the reaction. The resulting bubbles disrupt the flow in the microchannels causing the poor reactor performance shown in Fig. 8a.

4.2.6. Influence of catalyst formulation

Figs. 7 and 8 show that increasing the catalyst loading and reaction temperature are not feasible means of improving the reaction rate in the microreactor. Previous work [22] reported that grafting amino groups on CsX could enhance the catalyst activity for Knoevenagel condensation reaction. Experiments show that NH_2–CsX is roughly three times more active than the starting CsX catalyst. Fig. 6d plots the percent product yield for NaA membrane-0.01 g/cm^3 CsX and NaA membrane-0.01 g/cm^3 NH_2–CsX plates. The experimental plots for the microreactor show that the NH_2–CsX-coated plate gives four times higher product yield compared to the plate coated with CsX catalyst. The figure also shows that for both catalysts, the membrane microreactor outperformed the microreactor. A 25% improvement in product yield was obtained using the membrane microreactor. The product yield increases from 15 to 20% for the CsX catalyst and 55–80% for the NH_2–CsX. Analysis of the permeate stream showed that only pure water

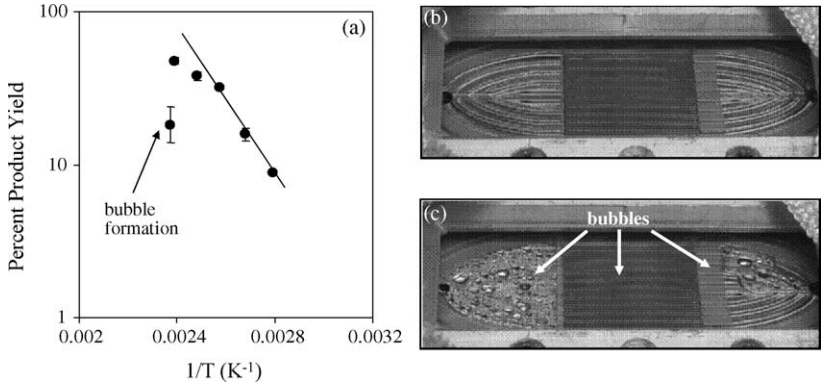

Fig. 8. (a) Plots of percent product yield as an inverse function of reaction temperature for a microreactor ($[C_7H_6O]_0$ = 4.8 M, $[ECA]_0$ = 4.8 M, catalyst loading = 0.03 g/cm^3 CsX, residence time = 0.8 h). The symbols and line represent the experimental and model data, respectively. Optical microscope pictures of the microreactor operating at temperatures of (b) 373 and (c) 423 K.

was pervaporated across the NaA zeolite membrane and calculations indicated that all water produced by the condensation reaction was completely removed by membrane pervaporation. Substituting the reaction rate equation for NH_2–CsX, the computational model provides a fair prediction of the experiment as shown in the figure.

4.2.7. Catalytic membrane plates

Model calculations indicated that locating the membrane closer to the catalyst layer could further enhance the performance of the membrane microreactor. Catalytic membranes were grown on each of the 35 microchannels in the catalytic membrane microreactor plate shown in Fig. 4. Grown in series, the composite membrane deposited on the microchannel wall consists of a continuous, seamless layer of 6 μm thick NaA zeolite and 4 μm thick Faujasite. The Faujasites deposited on top of NaA have a weight loading of 0.01 g/cm^3. A pure Faujasite membrane was not used because of its poor separation properties for water–benzaldehyde. Fig. 9 displays the reaction data obtained from the catalytic membrane plate after ion-exchange with cesium. The percent product yield from the microreactor reaches 80%, which is three times more than a microreactor with a similar weight loading of CsX catalyst. This is surprising given that the deposited Faujasites also contained the less active Y zeolite and the denser catalyst layer offered greater transport resistance. Also, the 80% product yield is higher than the equilibrium value of 72%. One possible explanation is that the composite structure of the catalytic membrane and the close proximity of the catalyst layer to NaA, which has a strong adsorbency for water, facilitated the rapid removal of water from the reaction resulting in the enhanced performance. Fig. 9 shows that a 91% product yield can be obtained under membrane microreactor operation, which is a significant improvement compared to the membrane–catalyst plates. However, the catalytic membrane failed and a leak was observed after 100 h of operation. Inspection showed that several of the micromembranes suffered cracks and damages. This may be caused by the uneven expansion of the composite layers of NaA and Faujasite during heating. Also, the catalytic micromembranes are exposed to shear caused by liquid flow in the microchannels.

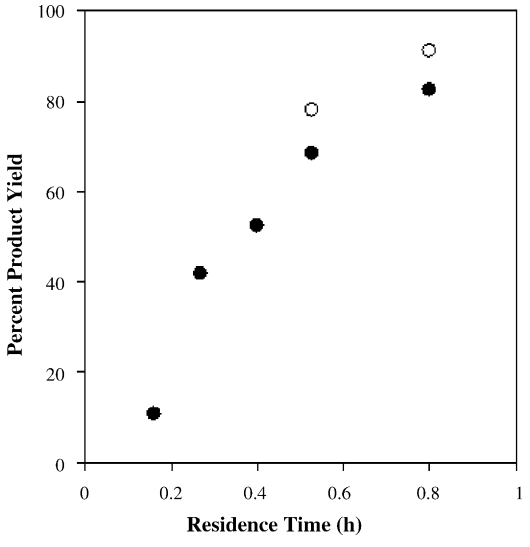

Fig. 9. Plots of percent product yield as a function of residence time for a catalytic membrane plate. (T = 373 K, $[C_7H_6O]_0$ = 4.8 M, $[ECA]_0$ = 4.8 M, catalyst loading = 0.01 g/cm^3 CsX–CsY, membrane = 6 μm NaA) The solid and open symbols represent the experimental data for the microreactor and membrane microreactor.

5. Concluding remarks

This work successfully miniaturized two types of membrane reactors, the packed-bed membrane reactor (PBMR) and catalytic membrane reactor (CMR). The membrane–catalyst plates with catalyst-coated microchannels and membrane separation layer approximate a PBMR. The membrane–catalyst plate is a more flexible design, where the catalyst and membrane can be separately optimized to provide the best performance. Catalytic membrane reactors often perform better than PBMR, but are more difficult to prepare since the membrane must exhibit both good catalytic and separation properties. The composite NaA–Faujasite micromembrane successfully combined the good catalytic properties of Cs–Faujasite for Knoevenagel condensation reaction and the excellent separation properties of NaA membrane for water resulting in an enhanced performance. A computational model based on established chemical engineering principles gave accurate prediction of the microreactor behavior and performance. The model described an optimum membrane microreactor as having narrow channels coated with a thin, uniform layer of catalyst with the membrane layer located immediately next to the catalyst. A selective separation membrane with a water permeation rate equivalent to the water production rate in the reactor is sufficient to achieve supra-equilibrium conversion in the membrane microreactor. Practical limitations to the membrane microreactor design and operations were imposed primarily by the thermodynamics and fluid properties of the reaction mixture. The volatility of the ethyl cyanoacetate and water means bubble formation in the microchannel. The bubbles cause cavitation that can be difficult to overcome. This places a lower limit to the size of microchannel as well as the maximum operating temperature. The material properties and synthesis methodology restrict the highest amounts of cesium atoms and amino groups that could be incorporated in the zeolite catalyst and therefore on the catalyst activity. The membrane thickness is dictated by the growth characteristic of the zeolite film. Thicker film is needed to obtain a defect-free ZSM-5 membrane because of the zeolite's columnar crystal shape.

Acknowledgements

The authors would like to thank the Hong Kong Research Grant Council (HKUST6009/02P) for funding this research. We also thank the help of the Material Preparation and Characterization Facility (MCPF) of Hong Kong University of Science and Technology.

References

[1] K.F. Jensen, Chem. Eng. Sci. 56 (2001) 293.
[2] D. Gobby, P. Angeli, A. Gavriilidis, J. Micromech. Microeng. 11 (2001) 126.
[3] O. Wörz, K.P. Jäckel, Th. Richter, A. Wolf, Chem. Eng. Sci. 56 (2001) 1029.
[4] R. Srinivasan, I.M. Hsing, P.E. Berger, K.F. Jensen, S.L. Firebaugh, M.A. Schmidt, M.P. Harold, J.J. Lerou, J.F. Ryley, AIChE J. 43 (1997) 3059.
[5] S.K. Ajmera, M.W. Losey, K.F. Jensen, M.A. Schmidt, AIChE J. 47 (2001) 1639.
[6] A. Gavriilidis, P. Angeli, E. Cao, K.K. Yeong, Y.S.S. Wan, Trans. IChemE 80A (2002) 3.
[7] A.Y.L. Leung, K.L. Yeung, Chem. Eng. Sci. 59 (2004) 4809.
[8] S.M. Lai, R. Martin-Aranda, K.L. Yeung, Chem. Commun. 2 (2003) 218.
[9] M.A. Salomón, J. Coronas, M. Menéndez, J. Santamaría, Appl. Catal. A 200 (2000) 210.
[10] E.V. Rebrov, G.B.F. Seijger, H.P.A. Calis, M.H.J.M. de Croon, C.M. van den Bleek, J.C. Schouten, Appl. Catal. A 206 (2001) 125.
[11] Y.S.S. Wan, J.L.H. Chau, A. Gavriilidis, K.L. Yeung, Chem. Commun. 8 (2002) 878.
[12] Y.S.S. Wan, A. Gavriilidis, K.L. Yeung, Trans. IChemE 81 (2003) 753.
[13] X.F. Zhang, S.M. Lai, R. Martin-Aranda, K.L. Yeung, Appl. Catal. A 261 (2004) 109.
[14] J.L.H. Chau, A.Y.L. Leung, K.L. Yeung, Lab-on-a-Chip 3 (2003) 53.
[15] J.L.H. Chau, A.Y.L. Leung, M.B. Shing, K.L. Yeung, C.M. Chan, Z. Tang, P. Sheng (Eds.), Nano Science and Technology: Novel Structure and Phenomena, Taylor and Francis, London, 2003, pp. 228–232.
[16] J.L.H. Chau, K.L. Yeung, Chem. Commun. 9 (2002) 960.
[17] Y.S.S. Wan, J.L.H. Chau, A. Gavriilidis, K.L. Yeung, Micropor. Mesopor. Mater. 42 (2001) 157.
[18] J.L.H. Chau, Y.S.S. Wan, A. Gavriilidis, K.L. Yeung, Chem. Eng. J. 88 (2002) 187.
[19] J. Coronas, J. Santamaria, Chem. Eng. Sci. 59 (2004) 4879.
[20] S.M. Lai, R. Martin-Aranda, K.L. Yeung, Chem. Commun. 2 (2003) 218–219.
[21] S.M. Lai, C.P. Ng, R. Martin-Aranda, K.L. Yeung, J. Micropor. Mesopor. Mater. 66 (2003) 239.
[22] Y.S.S. Wan, K.L. Yeung, A. Gavriilidis, Appl. Catal. A 281 (2005) 285.
[23] D.J. Quiram, I.M. Hsing, A.J. Franz, K.F. Jensen, M.A. Schmidt, Chem. Eng. Sci. 55 (2000) 3065.
[24] J.M. Commenge, L. Falk, J.P. Corriou, M. Matlosz, AIChE J. 48 (2002) 345.
[25] I.M. Hsing, R. Srinivasan, M.P. Harold, K.F. Jensen, M.A. Schmidt, Chem. Eng. Sci. 55 (2000) 3.
[26] E.V. Rebrov, M.H.J.M. de Croon, J.C. Schouten, Chem. Eng. Sci. 90 (2002) 61.
[27] W.M. Rohsenow, J.P. Harnett, Y.I. Cho (Eds.), Handbook of Heat Transfer, McGraw Hill, New York, 1998.
[28] H.G. Karge, J. Weitkamp, Molecular Sieves — Science and Technology: Synthesis, vol. 1, Springer, Berlin, 1998.
[29] S.M. Lai, L.T.Y. Au, K.L. Yeung, Micropor. Mesopor. Mater. 54 (2002) 63.
[30] A. Corma, V. Fornes, R.M. Martin-Aranda, H. Garcia, J. Primo, Appl. Catal. 59 (1990) 237.
[31] J.R. Welty, C.E. Wicks, R.E. Wilson, Fundamentals of Momentum, Heat, and Mass Transfer, Wiley, New York, USA, 1984.
[32] J.A. Wesselingh, R. Krishna, Mass Transfer in Multicomponent Mixtures, Delft University Press, Delft, The Netherlands, 2000.
[33] H.S. Fogler, Elements of Chemical Reaction Engineering, Prentice-Hall, Upper Saddle River, USA, 1992.
[34] N. Wakao, S. Kaguei, Heat and Mass Transfer in Packed Beds, Gordon and Breach Science Publishers, New York, USA, 1982.